Article:
Sengokmen Ozsoz, N. orcid.org/0000-0002-2000-7408, Pashneh-Tala, S. and Claeyssens, F. orcid.org/0000-0002-1030-939X (2024) Optimization of a high internal phase emulsion-based resin for use in commercial vat photopolymerization additive manufacturing. 3D Printing and Additive Manufacturing, 11 (2). pp. 496-507. ISSN 2329-7662

https://doi.org/10.1089/3dp.2022.0235

Final publication is available from Mary Ann Liebert, Inc.: https://doi.org/10.1089/3dp.2022.0235

Optimization of a High Internal Phase Emulsion (HIPE) based resin for use in commercial vat photopolymerization additive manufacturing

Nihan Sengokmen Ozsoz [1], Samand Pashneh-Tala [1], and Frederik Claeyssens[1*]

[1]*Department of Materials Science and Engineering, Kroto Research Institute, The University of Sheffield, Sheffield, United Kingdom*

[*]*f.claeyssens@sheffield.ac.uk*

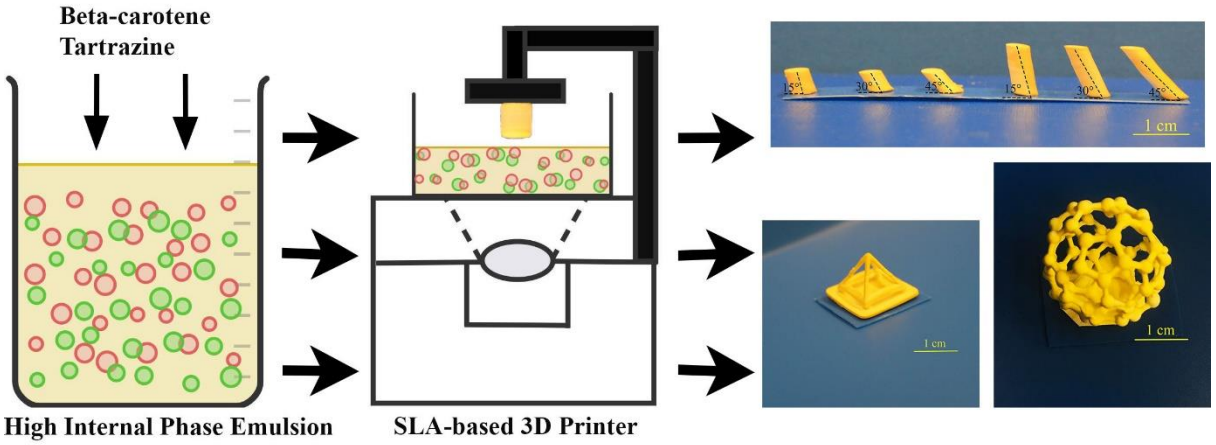

Final publication is available from Mary Ann Liebert, Inc.: https://doi.org/10.1089/3dp.2022.0235

Abstract

High internal phase emulsions (HIPEs) are potential stereolithography-based resins for producing innovative lightweight porous materials; however, the use of these resins has only been shown in bespoke stereolithography setups. These studies indicated that HIPEs tend to scatter the light during structuring via stereolithography, and can produce poorly defined, and low-resolution structures, but the inclusion of light absorbers can drastically increase the printing resolution. In this study, we focused on the inclusion of biocompatible light absorbers within the resin and the compatibility of those resins with a commercial vat photopolymerization additive manufacturing (or stereolithography) setup. A surfactant (hypermer) stabilized water-in-oil emulsion based on 2-ethylhexyl-acrylate and isobornyl-acrylate was used. For the light absorbers, both hydrophobic (beta-carotene) and hydrophilic (tartrazine) molecules were used, which dissolve in the organic phase and aqueous phase, respectively. It was found that using a combination of both beta-carotene and tartrazine provided the best stereolithography-based 3D printing resolution. Additionally, the emulsion was stable for the duration of the printing process and showed a porous polyHIPE structure with open surface porosity. The formulation of these HIPE-based resins permits them to be used in a wide range of applications since complex structures could be fabricated from HIPEs.

Keywords: *PolyHIPE, Vat photopolymerization, Stereolithography, 3D printing, Light absorber*

Final publication is available from Mary Ann Liebert, Inc.: https://doi.org/10.1089/3dp.2022.0235

1. Introduction

From the 1990s onwards, there has been an increased interest in the manufacture of porous polymer structures because of their flexibility of design, and relatively easy and low-cost manufacture [1–6]. Primarily, research in porous polymers focused on producing polymers with tunable physical properties, well-defined tunable porosities from micrometer to millimeter size and high surface areas. This led to a variety of potential applications, for example, filter materials, catalyst support, or scaffold materials in tissue engineering and 3D cell culture [1,7]. Porous polymers can also be used as templates for the manufacturing of porous metals, ceramics, carbons, and composites [1].

One versatile technique to produce porous polymers is emulsion templating where an emulsion of a pre-polymer or polymer solution continuous phase is combined with water as dispersed phase. During the process the polymer sets, and the water is removed to obtain the remaining polymer network template formed by the emulsion. When using large amounts of internal phase (over 74% of the total volume) and a suitable emulsifying surfactant, this process produces High Internal Phase Emulsions (HIPEs) [1,8–10]. These are templates to produce highly porous polymer structures (polyHIPEs) with potentially interconnected porosity [1,11]. PolyHIPEs can be shaped via traditional manufacturing techniques such as casting (molding) to make structures with low design complexity and flexibility, where post-processing can be applied to create complex structures [12,13]. An interesting novel route to shape polyHIPEs is via combining emulsion templating with additive manufacturing. This allows single-step manufacturing of inherently porous and lightweight complex structures with little to no post-processing [14–16].

Currently, additive manufacturing is emerging as an industrial manufacturing technique to fabricate three-dimensional objects directly from computer-aided design (CAD) files through layer-by-layer manufacturing, originally invented in the 1980s [17,18]. Additive manufacturing is

Final publication is available from Mary Ann Liebert, Inc.: https://doi.org/10.1089/3dp.2022.0235

a general term for a group of technologies, also known by the public as 3D printing. Additive manufacturing technologies are mainly divided into seven categories according to the terminology set out by ISO/ASTM 52900: 2015 [18,19]. These categories are binder jetting, directed energy deposition, material jetting, powder bed fusion, sheet lamination, material extrusion, and vat photopolymerization. Material extrusion (fused deposition modelling) and vat photopolymerization (stereolithography) are used for the additive manufacturing of polymer materials and have both been used to build porous polyHIPE 3D structures [14–16,20–22]. In these studies, bespoke emulsions were prepared by mixing water with suitable monomers, surfactants, crosslinkers, and photoinitiators and were printed on experimental in-house setups [18,23]. However, to our knowledge, their printability in commercial stereolithography-based 3D printers has not been demonstrated.

Even though additive manufacturing allows the manufacturing of complex polyHIPE structures, HIPE-based resins tend to scatter light during structuring via stereolithography [16]. Therefore, this can cause the production of poorly defined, low-resolution structures. Improving the resolution by using light absorbers has previously been reported by Choi and Wicker in standard non-porous stereolithography resins [24], and by Sherborne et al. in emulsion-based resins [16]. Sherborne et al. used Tinuvin 234 as a light absorber to reduce the resolution in a house-built stereolithography set-up to 200 µm for HIPE-based inks by reducing the light scattering arising in the focal point. Additionally, it was observed that the surface of the structures without light absorbers was non-porous, which was attributed to surface skin from the poorly cured polymer in the scattering region. The surface skin reduced the functionality of the structures, especially in applications that depend on surface porosity (e.g., cell culture scaffolds).

In this study, the use of high internal phase emulsions as potential 3D printing resins for producing inherently porous structures with a commercial vat photopolymerization-based 3D

Final publication is available from Mary Ann Liebert, Inc.: https://doi.org/10.1089/3dp.2022.0235

printer (Kudo 3D Titan2 HR) was investigated. This set-up integrates a 405 nm LED source and a DLP projector to project high-resolution images (up to 25 μm) on a 10.2 cm × 7.4 cm build platform [25]. It illuminates the sample from the bottom through a transparent base and a thin layer of uncured resin on the z-translation platform (bottom-up setup). In this bottom-up setup, there are 3 steps: a curing step, a pull-off step where the z-platform translates to pull the reacted resin from the transparent base, and a third step where the build platform moves back to produce the next layer. This convoluted sequence of steps for each layer could have significant consequences for emulsion stability and porosity, and this has been studied in detail in this publication.

We aimed to investigate the effects of two light absorbers on mainly the printing resolution and porous microstructure. Beta-carotene and tartrazine were used, which are biocompatible light absorbers, as highlighted in previous literature [26]. Beta-carotene is a hydrophobic compound, while tartrazine is hydrophilic. Accordingly, beta-carotene resides in the organic phase, whereas tartrazine is retained in the aqueous phase. This study explores the overall effects of hydrophobic and hydrophilic light absorbers in these emulsions and determines whether employing both together has any advantages over using each one separately.

Final publication is available from Mary Ann Liebert, Inc.: https://doi.org/10.1089/3dp.2022.0235

2. Materials and Methods

2.1. Materials

2-ethylhexyl acrylate (EHA), isobornyl acrylate (IBOA), trimethylolpropane triacrylate (TMPTA), 2 different forms of photoinitiators; diphenyl (2,4,6- trimethyl benzoyl)-phosphine oxide (in crystal form) and 2-hydroxy-2-methyl propiophenone (in liquid form), beta-carotene (synthetic, ≥93% (UV), powder), and tartrazine (dye content ≥85 %) were all purchased from Sigma Aldrich. The surfactant Hypermer B246-SO-M was kindly donated by Croda.

2.2. Methods

2.2.1. Preparation of High Internal Phase Emulsions

37.30 wt% 2-ethylhexyl acrylate (EHA), 37.30 wt% isobornyl acrylate (IBOA), 16.40 wt% trimethylolpropane triacrylate (TMPTA) (crosslinker), and 9.00 wt% Hypermer B246-SO-M (surfactant) were mixed to form the continuous organic phase. This mixture was heated using a heat gun until the surfactant was dissolved at 50°C. Afterwards, photoinitiators were added to the continuous phase at 2.5 wt% in crystal form and at 2.5 wt% in liquid form. The solution was heated to 40°C for 5 minutes to dissolve the photoinitiator, which is in crystal form.

HIPEs containing beta-carotene and tartrazine were fabricated by adding both to the continuous phase before the addition of the photoinitiator. Beta-carotene was added from 0.1 to 1.0 wt% (of the continuous phase), and tartrazine was added from 0.1 to 0.4 wt% (of the continuous phase) in increments of 0.1 wt% (Table 1).

Finally, 80 vol.% of distilled water, dH2O, (the internal phase) was added to the continuous phase to form an emulsion. The water was added dropwise while stirring the emulsion at 300 rpm (SciQuip-Pro 40 stirrer).

Final publication is available from Mary Ann Liebert, Inc.: https://doi.org/10.1089/3dp.2022.0235

Table 1. EHA, IBOA, TMPTA, hypermer, beta-carotene, and tartrazine ratio (wt%)

Samples	*Organic Phase*				*Light absorbers*	
	EHA (wt %)	*IBOA (wt %)*	*TMPTA (wt %)*	*Hypermer (wt %)*	*Beta-carotene*[a] *(wt %)*	*Tartrazine*[a] *(wt %)*
Pure	37.30	37.30	16.40	9.00	-	-
Beta-carotene	37.30	37.30	16.40	9.00	0.10 to 1.00	-
Tartrazine	37.30	37.30	16.40	9.00	-	0.10 to 0.40
Blend	37.30	37.30	16.40	9.00	0.40	1.00

[a]Beta-carotene and tartrazine concentration with respect to the organic phase

2.2.2. 3D Printing of High Internal Phase Emulsions

PolyHIPE structures were 3D printed using a commercially available, desktop 3D printer (Kudo 3D Titan2 HR). The 3D printer employed the vat polymerization technique and combined stereolithography (SLA) and digital light projection (DLP) methods using a 405 nm light source.

Computer-aided design (CAD) was used to produce the structures for 3D printing (SolidWorks 2018). These were formatted as .stl files and then prepared for 3D printing and sliced using Creation workshop (version 1.0.0.75).

2.2.2.1. 5×5 mm cylinders for the optimization of the light absorber content

Cylinder samples, 5 mm diameter × 5 mm height, were 3D printed and used to optimize the amounts of light absorbers in the emulsion. These cylinders contained 233 layers with a base and supports after slicing (see Supplementary Figure 1). Initially, the HIPE containing no beta-carotene or tartrazine, further denoted as “pure”, was used to 3D print the polyHIPE cylinders.

Final publication is available from Mary Ann Liebert, Inc.: https://doi.org/10.1089/3dp.2022.0235

Printing parameters (exposure time, lifting speed, lifting height, etc.) were varied to achieve the best 3D printing performance (the final parameters and overall print time are listed in Supplementary Table 1 and Table 18, respectively). After determining the most suitable 3D printing parameters for the pure HIPE, HIPEs including beta-carotene and tartrazine at varying concentrations were used to 3D print the polyHIPE cylinder structures. Additionally, the 3D printing parameters were modified slightly to achieve the best results when including the light absorbers (see Supplementary Tables 2-4,18). Once 3D printing was completed, the cylinders were washed with acetone to remove non-polymerized HIPE and then air-dried.

2.2.2.2. Investigation of the 3D printing resolution

Various calibration objects were 3D printed using the HIPEs to determine the resolution that could be achieved.

A calibration object including 5 mm-high posts of 3 mm, 2 mm, 1 mm, and 0.5 mm diameters was 3D printed from the pure HIPE and then from HIPEs that contained the optimized amounts of beta-carotene, tartrazine, and a blend (0.4% beta-carotene and 0.1% tartrazine) (see Supplementary Figure 4 and Tables 12-15, 18).

Additionally, cylinders, 5 mm diameter × 5 mm and 10 mm height, having 15°, 30°, and 45° inclines were also 3D printed from the pure HIPE and the HIPE containing the optimized amounts of beta-carotene, tartrazine, and a blend of them (see Supplementary Figures 2,3 and Tables 5-11, 18).

Final publication is available from Mary Ann Liebert, Inc.: https://doi.org/10.1089/3dp.2022.0235

2.2.2.3. Pyramid and Buckyball structures

3D designs of pyramid and buckyball structures were obtained from thingiverse.com [27,28]. These 3D-designed structures were fabricated from HIPEs containing a blend of beta-carotene and tartrazine to demonstrate the usability of HIPEs as 3D printing materials for producing complex geometric structures (see Supplementary Figures 5,6 and Tables 16-18).

2.2.3. Characterization of HIPEs and polyHIPEs

2.2.3.1. UV/Vis Spectrometer

A Jenway 6305 spectrophotometer was used to measure the light absorbance of the optimized amounts of the light absorbers at 405 nm. Beta-carotene was dissolved in the organic phase (hydrophobic compound), while tartrazine was dissolved in the aqueous phase (hydrophilic compound).

2.2.3.2. Scanning Electron Microscopy

A Tescan Vega3 Scanning Electron Microscopy (SEM) was used to image the cross-section and outer surface of 3D-printed polyHIPE samples. Before SEM imaging, samples were gold coated to provide conductivity (Edwards S150B sputter coater). Image J was used to measure pore diameters. 100 pores were measured for each sample to determine an average. A statistical correction factor of $2/\sqrt{3}$ was then applied to the results to account for the non-equatorial location of the pore diameter measurements [29,30].

Final publication is available from Mary Ann Liebert, Inc.: https://doi.org/10.1089/3dp.2022.0235

2.2.3.3. Helium Pycnometry

The porosity of the polyHIPEs was determined using helium pycnometry. PolyHIPE cylinders, 5 mm diameter × 5 mm height, were 3D printed from pure HIPE and from HIPEs that contained the optimized amounts of beta-carotene, tartrazine, and the blend (0.4% beta-carotene and 0.1% tartrazine). These cylinders were examined using an Accupyc 1340 Gas Pycnometer to calculate their porosity. The device determined the density and volume (V_{pyc}) of the samples. Equation 1 was used to calculate % porosity. V_{bulk} is the volume of the bulk cylinder sample.

$$\%\, porosity = \left(1 - \frac{\mathrm{Vpyc}}{\mathrm{Vbulk}}\right) \times 100 \quad (1)$$

Additionally, equivalent polyHIPE cylinders were also produced from UV-cured HIPEs, polymerized using a UV belt curer (GEW Mini Laboratory, GEW engineering UV) with a 100 W cm^{-2} UV bulb. Cylinders were cut from UV-cured polyHIPE samples using a 5 mm diameter hollow punch. UV-cured polyHIPE cylinders were produced from freshly prepared HIPEs and leftover HIPEs (which remained in the printing tank after 3D printing) to demonstrate the effect of the two-step up-and-down movement of the printing platform on porosity.

2.2.3.4. Statistical Analysis

All statistical analysis was undertaken in GraphPad Prism (version 8.4.3). One-way ANOVA with Tukey's multiple comparison analysis was applied to assess significant differences. Differences were considered significant when $p<0.0001$. All experiments were repeated three times, and the number of replicates (n) is mentioned in the figure legend.

Final publication is available from Mary Ann Liebert, Inc.: https://doi.org/10.1089/3dp.2022.0235

3. Results

3.1. UV-Vis Spectrometer

We aimed to formulate a resin that had a similar amount of light absorbance in the organic phase compared to the aqueous phase and to subsequently fine-tune the light absorbance within the respective phases via changing the concentration of the light absorber (beta-carotene and tartrazine) and observe any changes in shape fidelity and internal structure. To achieve this, the optical absorption of the two different absorbers beta-carotene and tartrazine was measured, and their absorptions were recorded at 405 nm for 8 different concentrations, between 2.5 µM and 20 µM with 2.5 µM intervals. From the gradient of these plots, (i.e., the experimental extinction coefficients at 405 nm) it can be calculated that tartrazine is in general 6.23× more absorbent at 405 nm than beta-carotene at the same molar concentration.

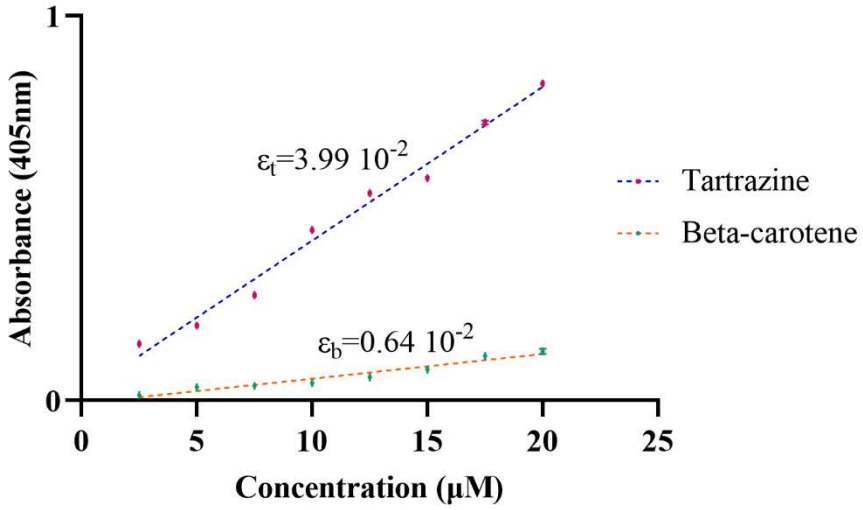

Figure 1. *Extinction coefficient graph of beta carotene and tartrazine samples at 405 nm (n=3)*

Final publication is available from Mary Ann Liebert, Inc.: https://doi.org/10.1089/3dp.2022.0235

Important to note is that both beta-carotene and tartrazine are natural products, which can have batch-to-batch variation (due to impurities) in their absorbance but also time-dependent variation, likely because of oxidation. For this reason, the extinction coefficient is regularly checked (Figure 1) and the concentrations of the light absorbers are adjusted accordingly to achieve consistent results.

3.2. Optimization of light absorber content and examination of 3D Printing resolution

Cylinder samples which were fabricated with different amounts of light absorbers, the diameter and height values, and the aspect ratio graph of 3D printed 5×5 mm cylinders were presented in Figure 2. These graphs were generated in GraphPad Prism (version 8.4.3).

The important figures to analyze were their diameter, height, and aspect ratio values, which are summarized in Figure 2. The shape fidelity of the print will likely be influenced by a few distinct and competing processes. As aforementioned, emulsion-based resins can scatter the light, which will translate into a larger object size both in the transversal and lateral directions of the printed stubs. The printed porous objects also exhibited shrinkage during the drying process after printing (see Supplementary Figure 7 and Table 19), which is a result of the water removal. Higher shrinkage will likely occur with under-cured objects because of lower cross-linking density. The results are highlighted in Figure 2. The results indicate that the inclusion of both beta-carotene and tartrazine influences the height, width, and aspect ratio of the printed structures. The printed cylinders included 1 mm spacer struts to easily disconnect the cylinder from the base (see Supplementary Figure 1). This allows for over-curing to occur in the z-direction, and this is observed in the cylinder cured without any light absorber (pure) (see Supplementary Figure 7). The aspect ratio varies non-linearly with increasing beta-carotene, indicating that the shape fidelity depends on a few competing factors as

Final publication is available from Mary Ann Liebert, Inc.: https://doi.org/10.1089/3dp.2022.0235

aforementioned. For both light absorbers, there was a maximum amount that could be added to the emulsion before print properties decreased. 1.0 wt % beta-carotene sample did not result in a successful print for beta-carotene, while 0.4 wt % of tartrazine addition resulted in a deteriorating structure.

Table 2. Diameter (mm), height (mm), and aspect ratio values

Samples	*Diameter (mm)*	*Height (mm)*	*Aspect Ratio*
Pure	4.73 ± 0.11	4.95 ± 0.02	0.96 ± 0.02
0.2 B	4.90 ± 0.04	4.84 ± 0.10	1.01 ± 0.01
0.4 B	4.89 ± 0.04	4.93 ± 0.05	0.99 ± 0.00
0.6 B	4.73 ± 0.06	4.94 ± 0.06	0.96 ± 0.02
0.8 B	4.53 ± 0.08	4.37 ± 0.01	1.04 ± 0.02
0.1 T	4.54 ± 0.04	4.68 ± 0.11	0.97 ± 0.03
0.2 T	4.20 ± 0.02	4.50 ± 0.19	0.93 ± 0.04
Blend	4.53 ± 0.09	4.60 ± 0.05	0.99 ± 0.03

Final publication is available from Mary Ann Liebert, Inc.: https://doi.org/10.1089/3dp.2022.0235

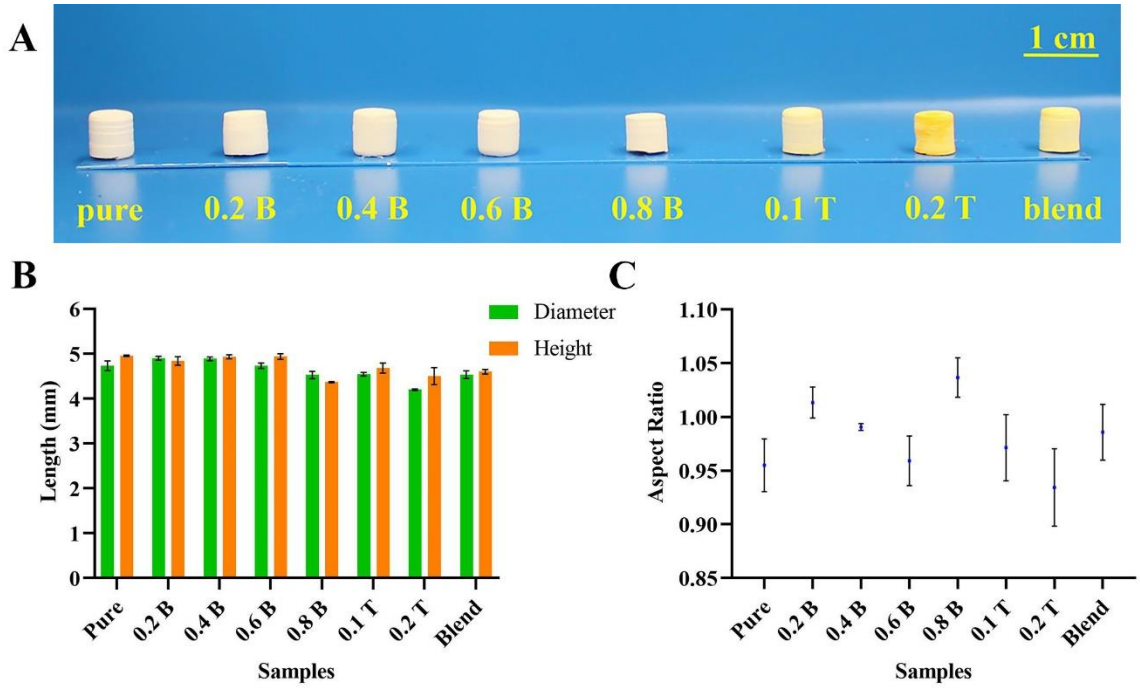

Figure 2. *(**A**) 3D printed 5×5 mm cylinders. (**B**) Diameter and height values of the 3D printed 5×5 mm cylinders. (**C**) The aspect ratio of the 3D printed 5×5 mm cylinders. (n=3)*

Overall, the 0.4 % beta-carotene allowed the manufacturing of structures that were closest to 3D design. The cylinder samples containing 0.4% beta-carotene have a diameter of 4.89 ± 0.04 mm and a height of 4.93 ± 0.05 mm (n=3) while the 3D model of the cylinder is 5×5 mm height. Also, the object with the aspect ratio closest to 1 is the 0.4 % beta-carotene structure. The 0.2 % beta-carotene structure is near second best with an aspect ratio was 1.01 ± 0.01 and diameter of 4.90 ± 0.04 mm and a height of 4.84 ± 0.10 mm. We also investigated the addition of tartrazine to the aqueous phase of the HIPE. In this series, the 0.1% tartrazine provided the best results (aspect ratio is 0.97 ± 0.03). Additionally, the combination of both was investigated by combining the best ones from each category. Interestingly, the blend samples exhibited shape fidelity with an aspect ratio of 0.99 ± 0.03 even though both their diameter (4.53 ± 0.09 mm) and height (4.60 ± 0.05 mm) were lower than the pure and beta-carotene samples. The observed

Final publication is available from Mary Ann Liebert, Inc.: https://doi.org/10.1089/3dp.2022.0235

shrinkage might indicate a lower cross-linking density in the polymer phase due to absorbance and is mainly observed in the emulsions that include tartrazine (Table 2).

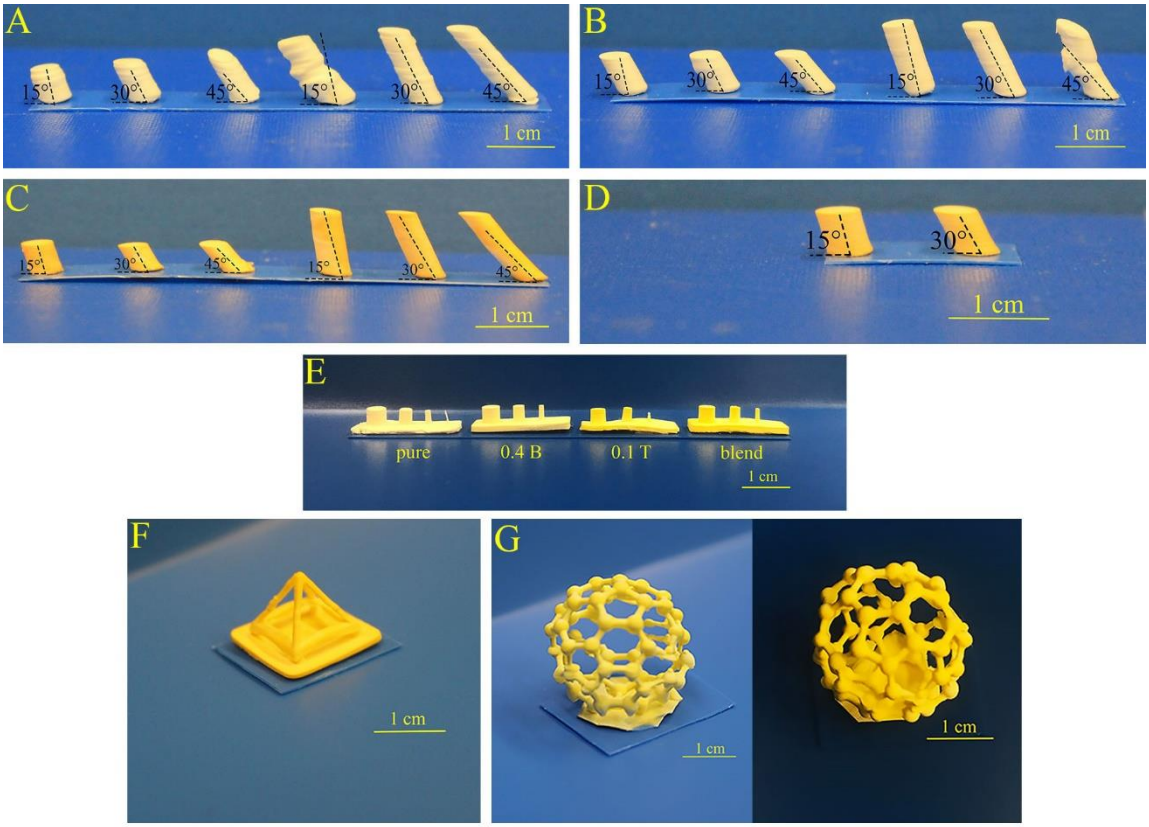

Figure 3. *(**A**) 3D printed cylinders having 5 mm and 10 mm height, and 15°, 30°, and 45° inclines from pure HIPE. (**B**) 3D printed cylinders having 5 mm and 10 mm height, and 15°, 30°, and 45° inclines from HIPE that contained 0.4 % beta-carotene. (**C**) 3D printed cylinders having 5 mm and 10 mm height, and 15°, 30°, and 45° inclines from HIPE that contained blend (0.4 % beta-carotene and 0.1 % tartrazine). (**D**) 3D printed cylinders having 5 mm height, and 15° and 30° inclines from HIPE that contained 0.1 % tartrazine. (**E**) Calibration object including 5 mm high posts of 3 mm, 2 mm, 1 mm, and 0.5 mm diameters which was 3D printed from pure HIPE and HIPEs that contained 0.4 % beta-carotene, 0.1 % tartrazine, and blend (0.4 % beta-carotene and 0.1 % tartrazine), respectively. (**F**) 3D printed pyramid structure from HIPE that contained blend (0.4 % beta-carotene and 0.1 % tartrazine). (**G**) 3D printed buckyball structure from HIPE that contained blend (0.4 % beta-carotene and 0.1 % tartrazine).*

A second test was how well overhangs are recreated in polyHIPE 3D printing. For this purpose, various cylinder structures having 5 mm and 10 mm height, and 15°, 30°, and 45° inclines were

Final publication is available from Mary Ann Liebert, Inc.: https://doi.org/10.1089/3dp.2022.0235

printed and presented in Figure 3. As a result, although these cylinder structures were created from pure, beta-carotene, and blend categories, only the cylinders having 5 mm height and 15° and 30° inclines were obtained in the tartrazine category.

The 3D-printed structures were examined in terms of resolution, and the best resolution was obtained from the blend light absorber category. All 6 cylinders were 3D printed without any distortion and over-curing in the structure. On the other hand, pure polyHIPE cylinders presented the least optimal results due to their distorted, over-cured structure with a prominent layered appearance arising from the printing process. Even though the cylinders containing 0.4 % beta-carotene showed similarity with pure polyHIPE cylinders, they presented more uniform structures except for the sample having 10 mm height and 45° incline. However, the layered structure caused by printing was noticeable, though to a lesser extent compared to the pure cylinders. Unlike pure and 0.4 % beta-carotene, the cylinders that contained 0.4 % beta-carotene and the blend did not show any distorted or layered structure. Finally, only 2 cylinders having 5 mm height and 15° and 45° incline were 3D printed from the HIPEs containing 0.1 % tartrazine although they were as uniform as the cylinders containing blend. As the height and incline of the cylinders increased, the attachment of the printed objects to the printing platform decreased, and the cylinders dropped from the printing platform during the 3D printing process. For this reason, the other cylinders failed.

Figure 3E presents a series of 3D printed calibration objects, including 5 mm high posts of 3 mm, 2 mm, 1 mm, and 0.5 mm diameters. The 0.5 mm width post could only be seen in the calibration object of pure polyHIPE, and it could not be printed with the others. This is likely due to the tendency of scattering-induced over-curing in pure HIPE. Even though the over-curing of HIPEs is a problem when fabricating more complex designs, it may be advantageous when fabricating the fine details. Except for the 0.5 mm post, the posts could be 3D printed from HIPEs containing 0.4% beta-carotene and the blend, while the 1 mm width post was

Final publication is available from Mary Ann Liebert, Inc.: https://doi.org/10.1089/3dp.2022.0235

incomplete in 0.1 % tartrazine. The pyramid structure containing inclined and thin edges (1.10 mm in the design file) and the buckyball structure including thin small spheroids (2 mm in the design file) connected by thin lines (0.90 mm in the design file) were 3D printed as proof of the usability of HIPEs to fabricate more complicated structures.

3.3. Comparison of the porous structures of the polyHIPEs containing different amounts of light absorbers

The layered microstructure caused by the 3D printing process of the polyHIPEs is presented in Figure 4(A-D). Layers and the interconnectivity between layers could be seen clearly. 6 layers from each category were measured, and the layer thicknesses were 30.35 ± 0.55 µm, 29.65 ± 0.65 µm, 29.40 ± 0.75 µm, and 29.70 ± 0.70 µm for pure, 0.4 % beta-carotene, 0.1% tartrazine, and blend, respectively (Figure 4K). These results also matched the z-layer thickness (30 µm) that was created by the slicing of the 3D model, and consequently the z-translation step of the z-stage.

After analyzing the effects of light absorbers on the resolution, we focused on investigating their effects on the pore structure since the degree of porosity and pore size are crucial properties in these materials, which directly affect the application area. PolyHIPEs that contained 0.4 % beta-carotene, 0.1 % tartrazine, the blend, and pure polyHIPE were investigated in terms of the degree of porosity and pore size. Also, to fully understand the influence of the printing process on the internal structure of the polyHIPEs, the pore size and porosity within 3D-printed structures were examined. The data were compared with the measured pore size and porosity in a fresh batch of UV-cured polyHIPEs and with a sample taken out of the resin tank after the printing process was completed (UV-cured leftover). These

Final publication is available from Mary Ann Liebert, Inc.: https://doi.org/10.1089/3dp.2022.0235

data are summarized in Table 3 and Figures 4 and 5 and provide the following interesting insight into the printing process.

Table 3. Pore size (µm), porosity (%), and layer thickness (µm)

Samples		*Pore Size (µm)*	*Porosity (%)*	*Layer Thickness (µm)*
3D-printed	Pure	13.97 ± 3.13	70.59 ± 2.62	30.35 ± 0.55
	0.4 B	15.27 ± 3.31	70.70 ± 1.14	29.65 ± 0.65
	0.1 T	18.75 ± 5.76	64.17 ± 4.58	29.40 ± 0.75
	Blend	18.36 ± 2.60	67.47 ± 2.09	29.70 ± 0.70
UV-cured fresh	Pure	37.05 ± 3.85	82.50 ± 0.57	n/a
	0.4 B	29.15 ± 4.35	80.58 ± 2.06	n/a
	0.1 T	32.25 ± 3.86	81.29 ± 2.10	n/a
	Blend	40.82 ± 6.18	80.77 ± 1.69	n/a
UV-cured	Pure	21.39 ± 2.56	76.65 ± 1.40	n/a
	0.4 B	14.87 ± 2.73	70.20 ± 3.03	n/a

Focusing on the pore size within the 3D-printed objects first, the pore sizes of the pure, 0.4 % beta-carotene, 0.1 % tartrazine, and the blend samples were 13.97 ± 3.13 µm, 15.27 ± 3.31 µm, 18.75 ± 5.76 µm, and 18.36 ± 2.60 µm, respectively, indicating that the pure polyHIPE sample had the smallest pores while the 0.1 % tartrazine sample had the largest pore size. On the other hand, the similarity in the pore sizes of 0.1 % tartrazine sample and the blend sample has been observed. Secondly, pure and 0.4 % beta-carotene samples showed more uniform pores than 0.1 % tartrazine samples based on their standard deviations as this could be seen in Table 3, whereas the blend exhibited more uniform pores.

Final publication is available from Mary Ann Liebert, Inc.: https://doi.org/10.1089/3dp.2022.0235

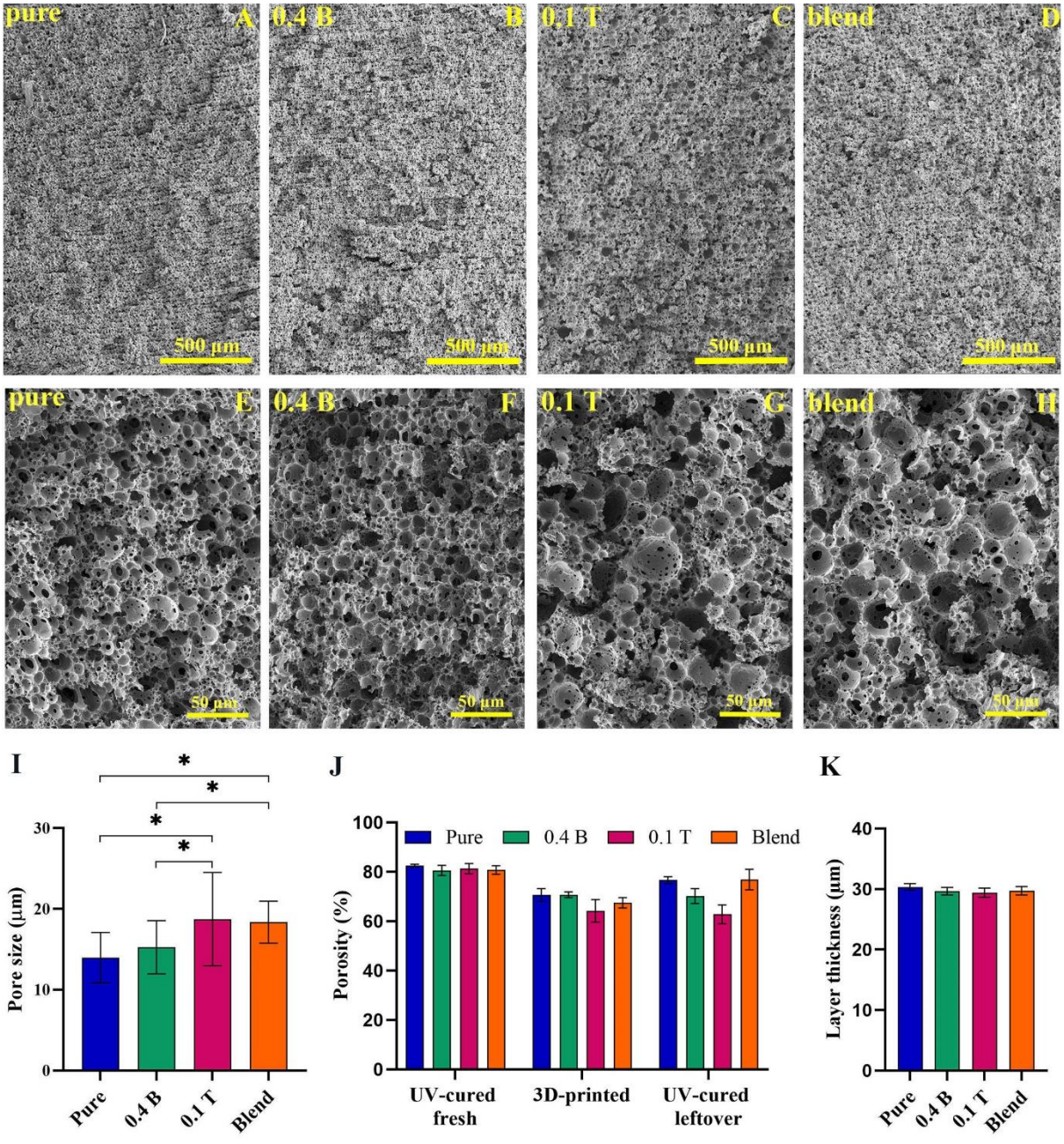

Figure 4. *Layer-by-layer structure of 3D printed polyHIPE samples,* ***(A)*** *pure polyHIPE,* ***(B)*** *polyHIPE containing 0.4 % beta-carotene,* ***(C)*** *polyHIPE containing 0.1 % tartrazine,* ***(D)*** *polyHIPE containing blend (0.4 % beta-carotene and 0.1 % tartrazine). Porous microstructure of 3D printed polyHIPE samples,* ***(E)*** *pure polyHIPE,* ***(F)****polyHIPE containing 0.4 % beta-carotene,* ***(G)*** *polyHIPE containing 0.1 % tartrazine,* ***(H)*** *polyHIPE containing blend (0.4 % beta-carotene and 0.1 % tartrazine).* ***(I)*** *Pore size vs Samples graph, *: significant difference (p<0.0001).* ***(J)*** *The comparison of the degree of porosity of UV-cured fresh, 3D-printed, and UV-cured leftover samples.* ***(K)*** *Layer thickness vs Samples graph. (n=3)*

Final publication is available from Mary Ann Liebert, Inc.: https://doi.org/10.1089/3dp.2022.0235

According to the statistical analysis (Figure 4I), the pore size of the 0.1 % tartrazine and the blend samples were compared with the pure and 0.4 % beta-carotene samples, and it was found that there was a statistically significant difference between them. On the other hand, there is no statistically significant difference between the pure and 0.4 % beta-carotene samples, and between 0.1 % tartrazine and the blend samples.

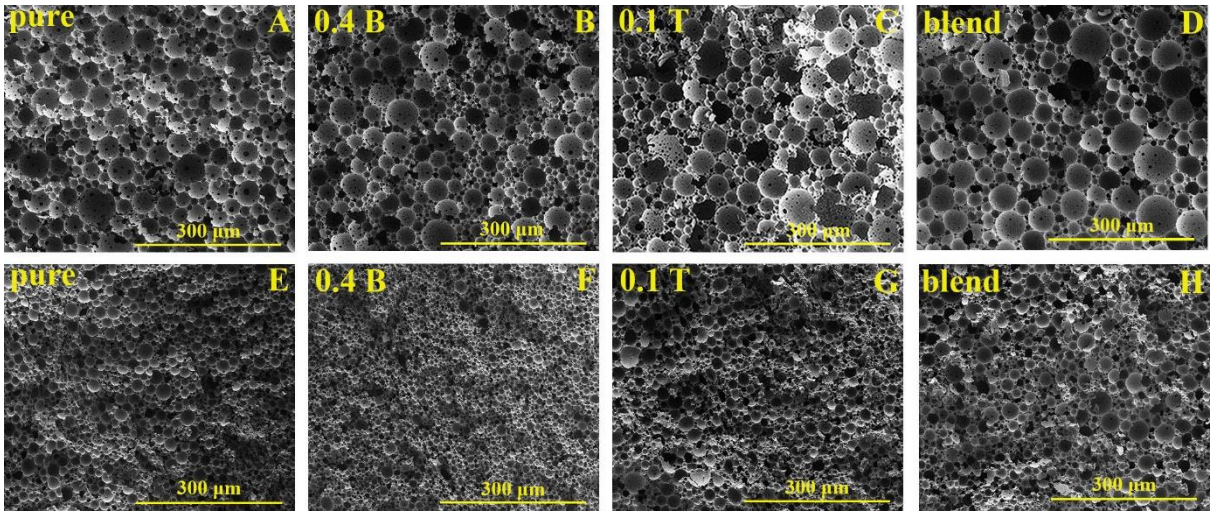

Figure 5. *Porous microstructure of UV-cured polyHIPE samples from fresh HIPEs,* ***(A)*** *pure polyHIPE,* ***(B)*** *polyHIPE containing 0.4 % beta-carotene,* ***(C)*** *polyHIPE containing 0.1 % tartrazine,* ***(D)*** *polyHIPE containing blend (0.4 % beta-carotene and 0.1 % tartrazine) and from leftover HIPEs,* ***(E)*** *pure polyHIPE,* ***(F)****polyHIPE containing 0.4 % beta-carotene,* ***(G)*** *polyHIPE containing 0.1 % tartrazine,* ***(H)*** *polyHIPE containing blend (0.4 % beta-carotene and 0.1 % tartrazine). (n=3)*

The porosity of the 3D-printed samples also showed a similar difference between the pure and beta-carotene-containing samples compared to the tartrazine-containing samples. The porosity drops to ~70% in the first group, while in the second group it drops to ~65%. Important to note is that this drop in porosity implies that the 3D HIPE emulsions do not produce polyHIPEs but rather lower porosity polyMIPEs (for Medium Internal Phase Emulsions). To discard the potential effect of closed surface porosity of the printed objects (see section 3.4) on the

Final publication is available from Mary Ann Liebert, Inc.: https://doi.org/10.1089/3dp.2022.0235

measurement, the porosity was re-measured on 3D-printed samples with their surface layers removed and no difference was observed.

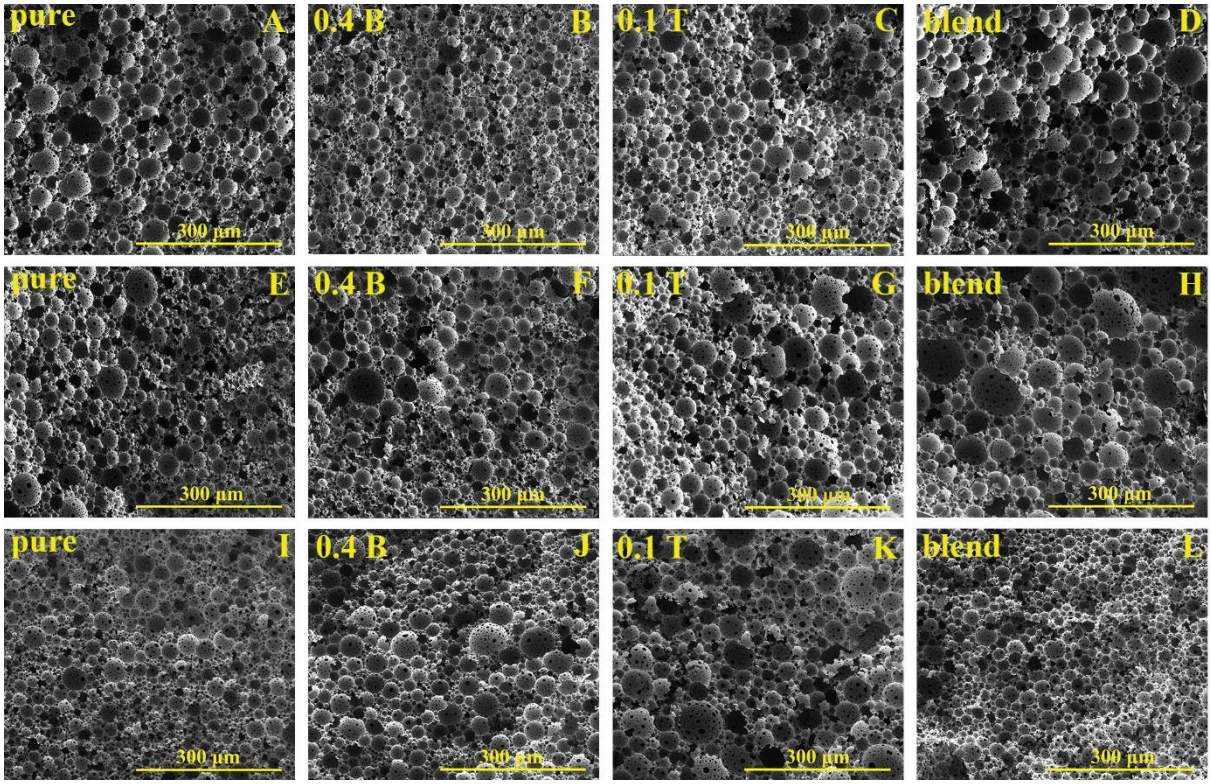

Figure 6. *Porous microstructure of UV-cured polyHIPE samples after 1 day* ***(A)*** *pure polyHIPE,* ***(B)*** *polyHIPE containing 0.4 % beta-carotene,* ***(C)*** *polyHIPE containing 0.1 % tartrazine,* ***(D)*** *polyHIPE containing blend (0.4 % beta-carotene and 0.1 % tartrazine), after 3 days* ***(E)*** *pure polyHIPE,* ***(F)****polyHIPE containing 0.4 % beta-carotene,* ***(G)*** *polyHIPE containing 0.1 % tartrazine,* ***(H)*** *polyHIPE containing blend (0.4 % beta-carotene and 0.1 % tartrazine), and after 7 days* ***(I)*** *pure polyHIPE,* ***(J)*** *polyHIPE containing 0.4 % beta-carotene,* ***(K)*** *polyHIPE containing 0.1 % tartrazine,* ***(L)*** *polyHIPE containing blend (0.4 % beta-carotene and 0.1 % tartrazine). (n=3)*

These results can be further compared to the results obtained from UV-cured polyHIPEs/MIPEs fabricated from fresh HIPEs and the emulsion that was left over in the resin tank after printing. The results can be summarized as follows: the leftover resin produced polyMIPEs with very similar pore size and porosity compared to the 3D-printed objects (in between 15-20 µm and 62-76% depending on the formulation), while the UV-cured fresh polyHIPEs exhibited larger

Final publication is available from Mary Ann Liebert, Inc.: https://doi.org/10.1089/3dp.2022.0235

pore sizes (in between 30-40 µm and 80-82% depending on the formulation). These differences can be explained by the different conditions the emulsions are exposed to during printing versus standard UV-curing. During 3D printing, the emulsion gets agitated by the up-and-down movement of the printing platform during the pull-off and curing steps causing a reduction in the pore size during curing.

Table 4. Pore sizes (µm) in day 1, day 3, and day 7

Samples	*Pore Size (µm)*		
	Day 1	*Day 3*	*Day 7*
Pure	36.90 ± 5.01	33.96 ± 5.50	32.86 ± 4.67
0.4 B	29.55 ± 5.09	33.44 ± 5.22	35.76 ± 6.88
0.1 T	32.43 ± 5.68	34.79 ± 5.88	42.59 ± 6.94
Blend	40.28 ± 7.11	39.23 ± 7.82	34.26 ± 6.28

Also, interesting to note is that the tartrazine-containing samples showed a higher reduction in porosity than the others. The addition of tartrazine decreased the porosity in addition to the up-and-down movement of the printing platform. Based on these findings, a 7-day emulsion stability test was performed, and the results are presented in Fig. 6 and Table 4. Even though the pore sizes of 0.4 % beta-carotene polyHIPEs and 0.1 % tartrazine polyHIPEs increased as time increased, the blend and pure polyHIPEs showed a slight decrease in their pore sizes as time increased.

Final publication is available from Mary Ann Liebert, Inc.: https://doi.org/10.1089/3dp.2022.0235

3.4. Surface Porosity

The outer surface of the cylinders was imaged via SEM to investigate the effects of light absorbers on the surface porosity. The pure and 0.4 % beta-carotene samples showed almost closed surfaces, whereas 0.1 % tartrazine and the blend samples provided porous surfaces. This indicated that oil-soluble (continuous phase) and water-soluble (internal phase) light absorbers have different effects on surface porosity and that only absorbers soluble in the internal phase ensure open surface porosity. This indicates that by including the light absorbers in the aqueous phase, the aqueous phase also absorbs the scattered light, which then reduces the occurrence of the poorly polymerized polymer boundary layer that gives rise to the polymer surface skin.

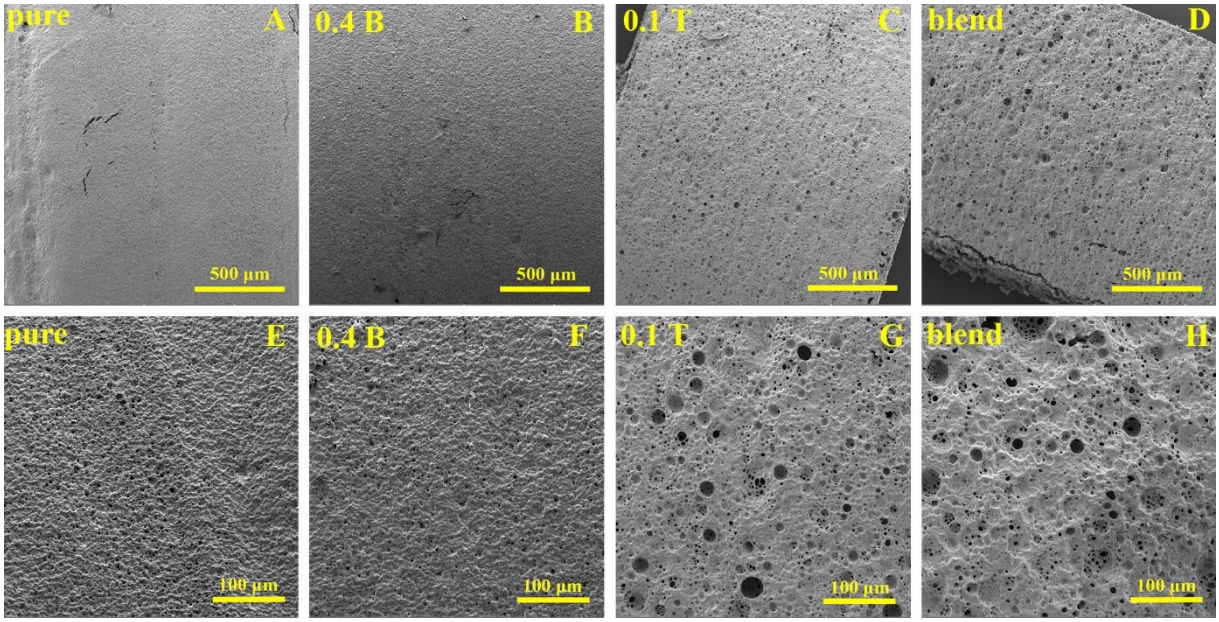

Figure 7. *The porosity of the outer surface of the 3D printed samples* ***(A&E)*** *pure polyHIPE,* ***(B&F)*** *polyHIPE contains 0.4 % beta carotene,* ***(C&G)*** *polyHIPE contains 0.1 % tartrazine,* ***(D&H)*** *polyHIPE contains 0.4 % beta carotene and 0.1 % tartrazine. (n=3)*

Final publication is available from Mary Ann Liebert, Inc.: https://doi.org/10.1089/3dp.2022.0235

4. Discussion

Current literature indicates that there is a noted increasing interest in the use of porous materials, particularly polyHIPEs, in various applications. Even though polyHIPEs are frequently proposed as materials for 3D cell culture and tissue engineering applications, they are also usable in different industrial applications by controlling their porous morphology, and physical and mechanical properties [1,31–35]. For the further adaptation of the polyHIPE technology in various industrial applications, these materials should also be able to be manufactured in a broad range of user-defined shapes. For this reason, manufacturing polyHIPEs via vat photopolymerization would be a convenient way since this process allows high-resolution fabrication.

Pure HIPEs were over-cured while fabricating cylinders with 5 mm and 10 mm heights and 15°, 30°, and 45° inclines. The reason for this over-curing is light scattering during the 3D printing process, as has been reported in the literature [36,37]. Light scattering could be reduced by including light absorbers within the resin, thus enabling the manufacture of objects with improved resolution via vat photopolymerization. For example, Tinuvin Carboprotect and Tinuvin 234 have been used as light absorbers to improve the resolution of 3D printed polyHIPEs, as reported by Susec et al. and Sherborne et al., respectively [16,38].

We achieved the best resolution using the blend light absorber (0.4 % beta-carotene and 0.1 % tartrazine). This allowed the 3D printing of a pyramid structure having inclined edges and a buckyball structure (Figure 3). Thus, we have manufactured the most complex structures to date obtained from HIPEs via stereolithography-based additive manufacturing thanks to the inclusion of the blend light absorber. Additionally, these structures could be manufactured with both internal and surface porosity, but interestingly, the pore size within the printed structures was smaller than a structure directly UV-cured from a fresh HIPE (15-20 μm compared to 30-

Final publication is available from Mary Ann Liebert, Inc.: https://doi.org/10.1089/3dp.2022.0235

40 µm, Figure 5 and Table 2), and the total porosity decreased by ~10%. This was likely due to a few different conditions the emulsion is exposed to during printing. Indeed, the print platform moves in a concerted up-and-down movement during printing to pull off the printed layer from the resin tank and move back to the set z-layer thickness of 30 µm for the next photopolymerization cycle. This restricts the pore size within the scaffolds to be smaller than 30 µm since the emulsion droplets need to fit in between the resin tank and the printed structure on the printing platform. Additionally, the agitation associated with the movement of the printing platform induces increased mixing and smaller pores throughout the resin, as indicated by the similar pore size observed in the leftover resin after printing. The overall stability of the resins at room temperature is at least 7 days, with only a slight change in pore size observed during this period (Figure 6 and Table 3).

An important additional factor is the appearance of a closed polymer layer on the surface of the 3D-printed structures that contain no light absorber. This has been previously reported by Sherborne et al. [16] and is due to a poorly polymerized surface layer that collapses as surface skin onto the 3D-printed objects after washing. This study reported that UV-234 (Tinuvin 234) produces an open surface pore structure. Similarly, our work indicated that the inclusion of tartrazine enables an open surface pore structure (Figure 7G-H) while the inclusion of beta-carotene results in a closed surface (Figure 7). This tunability of closed/open surface porosity by the inclusion of different light absorbers is likely interesting for various applications; for example, in tissue engineering, open surface porosity is preferred to enable cell ingrowth.

Final publication is available from Mary Ann Liebert, Inc.: https://doi.org/10.1089/3dp.2022.0235

5. Conclusion

To conclude, firstly, this study demonstrated that using the blend of beta-carotene and tartrazine as a light absorber considerably improves the 3D printing resolution for producing porous polymer structures. Thus, it allows the fabrication of more complex and detailed objects from HIPEs via stereolithography-based additive manufacturing. The blend of 0.4 wt% beta-carotene and 0.1 wt% tartrazine relative to the organic phase has been shown to preserve both the surface porosity and internal porosity of the 3D-printed objects. The pore size was reduced in the 3D-printed objects compared to the UV-cured fresh polyHIPEs, from ~30-40 to 15-20 μm. The overall porosity was also reduced, and the 3D-printed porous polymers can be classified as polyMIPEs rather than polyHIPEs. This study illustrated that 3D printing of intricate structures of porous polymers is possible with commercial stereolithography setups, which opens the route towards using this technology for a host of applications.

Final publication is available from Mary Ann Liebert, Inc.: https://doi.org/10.1089/3dp.2022.0235

Authors' Contributions

N.S.O. contributed to conceptualization, data curation, formal analysis, investigation, methodology, validation, visualization, writing—original draft preparation. S.P.T. contributed to conceptualization, methodology, visualization, writing—review and editing. F.C. contributed to conceptualization, methodology, project administration, supervision, visualization, writing—original draft preparation, writing—review and editing. All authors have read and agreed to the published version of the manuscript.

Conflicts of Interest

The authors declare no conflict of interest.

Acknowledgments

The authors gratefully acknowledge the Republic of Turkey-The Ministry of National Education for funding Nihan Sengokmen Ozsoz. The authors also would like to thank Mina Aleemardani for her help in taking photos of 3D printed objects.

Final publication is available from Mary Ann Liebert, Inc.: https://doi.org/10.1089/3dp.2022.0235

References

1. Silverstein MS. PolyHIPEs: Recent Advances in Emulsion-Templated Porous Polymers. Prog Polym Sci 2014;39(1):199–234; doi: 10.1016/j.progpolymsci.2013.07.003.

2. Ozdil D and Aydin HM. Polymers for Medical and Tissue Engineering Applications. J Chem Technol Biotechnol 2014;89(12):1793–1810.

3. Yang F, Zhao G, Zhou C, et al. Phase Change Materials (PCM) Based Cold Source for Selective Freezing 3D Printing of Porous Materials. Int J Adv Manuf Syst 2018;95(5):2145–2155; doi: 10.1007/s00170-017-1295-9.

4. Vanderesse N, Ky I, Quevedo González F, et al. Image Analysis Characterization of Periodic Porous Materials Produced by Additive Manufacturing. Mater Des 2016;92:767–778; doi: 10.1016/j.matdes.2015.12.062.

5. Liu Z, Zhan J, Fard M, et al. Acoustic Properties of a Porous Polycarbonate Material Produced by Additive Manufacturing. Mater Lett 2016;181:296–299; doi: 10.1016/j.matlet.2016.06.045.

6. Cameron NR. High Internal Phase Emulsion Templating as a Route to Well-Defined Porous Polymers. Polymer 2005;46(5):1439–1449; doi: 10.1016/j.polymer.2004.11.097.

7. Qian L and Zhang H. Porogen Incorporation and Phase Inversion. In: Porous Polymers. John Wiley and Sons: United Kingdom; 2011; pp. 79–117; doi: 10.1002/9780470929445.ch3.

Final publication is available from Mary Ann Liebert, Inc.: https://doi.org/10.1089/3dp.2022.0235

8. Lissant KJ and Mayhan KG. A Study of Medium and High Internal Phase Ratio Water/Polymer Emulsions. J Colloid Interface Sci 1973;42(1):201–208; doi: 10.1016/0021-9797(73)90025-8.

9. Lissant KJ, Peace BW, Wu SH, et al. Structure of High-Internal-Phase-Ratio Emulsions. J Colloid Interface Sci 1974;47(2):416–423; doi: 10.1016/0021-9797(74)90273-2.

10. Durgut E, Sherborne C, Aldemir Dikici B, et al. Preparation of Interconnected Pickering Polymerized High Internal Phase Emulsions by Arrested Coalescence. Langmuir 2022;38(36):10953–10962; doi: 10.1021/acs.langmuir.2c01243.

11. Aldemir Dikici B and Claeyssens F. Basic Principles of Emulsion Templating and Its Use as an Emerging Manufacturing Method of Tissue Engineering Scaffolds. Front Bioeng Biotechnol 2020;8:875; doi: 10.3389/fbioe.2020.00875.

12. Mu X, Bertron T, Dunn C, et al. Porous Polymeric Materials by 3D Printing of Photocurable Resin. Mater Horiz 2017;4(3):442–449; doi: 10.1039/c7mh00084g.

13. Sears NA, Dhavalikar PS and Cosgriff-Hernandez EM. Emulsion Inks for 3D Printing of High Porosity Materials. Macromol Rapid Commun 2016;37(16):1369–1374; doi: 10.1002/marc.201600236.

14. Johnson DW, Sherborne C, Didsbury MP, et al. Macrostructuring of Emulsion-Templated Porous Polymers by 3D Laser Patterning. Adv Mater 2013;25(23):3178–3181; doi: 10.1002/adma.201300552.

15. Owen R, Sherborne C, Paterson T, et al. Emulsion Templated Scaffolds with Tunable Mechanical Properties for Bone Tissue Engineering. J Mech Behav Biomed Mater 2016;54:159–172; doi: 10.1016/j.jmbbm.2015.09.019.

Final publication is available from Mary Ann Liebert, Inc.: https://doi.org/10.1089/3dp.2022.0235

16. Sherborne C, Owen R, Reilly GC, et al. Light-Based Additive Manufacturing of PolyHIPEs: Controlling the Surface Porosity for 3D Cell Culture Applications. Mater Des 2018;156:494–503; doi: 10.1016/j.matdes.2018.06.061.

17. Gardan J. Additive Manufacturing Technologies: State of the Art and Trends. Additive Manufacturing Handbook. 2017:149-168.

18. Pagac M, Hajnys J, Ma QP, et al. A Review of Vat Photopolymerization Technology: Materials, Applications, Challenges, and Future Trends of 3d Printing. Polymers 2021;13(4):598; doi: 10.3390/polym13040598.

19. ISO/ASTM 52900:2021 (en) Additive Manufacturing — General Principles — Fundamentals and vocabulary. Available from: https://www.iso.org/obp/ui/#iso:std:iso-astm:52900:ed-2:v1:en [Last accessed: 8/4/2022].

20. Sears N, Dhavalikar P, Whitely M, et al. Fabrication of Biomimetic Bone Grafts with Multi-Material 3D Printing. Biofabrication 2017;9(2):025020; doi: 10.1088/1758-5090/aa7077.

21. Wang AJ, Paterson T, Owen R, et al. Photocurable High Internal Phase Emulsions (HIPEs) Containing Hydroxyapatite for Additive Manufacture of Tissue Engineering Scaffolds with Multi-Scale Porosity. Mater Sci Eng C 2016;67:51–58; doi: 10.1016/j.msec.2016.04.087.

22. Park SH, Lim TW, Yang DY, et al. Fabrication of a Bunch of Sub- 30-Nm Nanofibers inside Microchannels Using Photopolymerization via a Long Exposure Technique. Appl Phys Lett 2006;89(17); doi: 10.1063/1.2363956.

Final publication is available from Mary Ann Liebert, Inc.: https://doi.org/10.1089/3dp.2022.0235

23. Taormina G, Sciancalepore C, Messori M, et al. 3D Printing Processes for Photocurable Polymeric Materials: Technologies, Materials, and Future Trends. J Appl Biomater Func Mater 2018;16(3):151–160; doi: 10.1177/2280800018764770.

24. Choi JW, Wicker RB, Cho SH, et al. Cure Depth Control for Complex 3D Microstructure Fabrication in Dynamic Mask Projection Microstereolithography. Rapid Prototyp J 2009;15(1):59–70; doi: 10.1108/13552540910925072.

25. Kudo 3D Printing Guide. Available from: https://www.dropbox.com/s/qs7c1w95drgmu1l/Kudo3D_Printing_Guide_v1.7.pdf?dl=0 [Last accessed: 8/4/2022].

26. Field J, Haycock JW, Boissonade FM, et al. A Tuneable, Photocurable, Poly(Caprolactone)-Based Resin for Tissue Engineering-Synthesis, Characterisation and Use in Stereolithography. Molecules 2021;26(5):1199; doi: 10.3390/molecules26051199.

27. Hollow(Er) Calibration Pyramid. Available from: https://www.thingiverse.com/thing:29429 [Last accessed: 10/26/2022].

28. C60 Carbon Fullerene Buckyball. Available from: https://www.thingiverse.com/thing:4077417 [Last accessed: 10/26/2022].

29. Carnachan RJ, Bokhari M, Przyborski SA, et al. Tailoring the Morphology of Emulsion-Templated Porous Polymers. Soft Matter 2006;2(7):608–616; doi: 10.1039/B603211G.

30. Pashneh-Tala S, Moorehead R and Claeyssens F. Hybrid Manufacturing Strategies for Tissue Engineering Scaffolds Using Methacrylate Functionalised Poly(Glycerol Sebacate). J. Biomater Appl 2020;34(8):1114-1130; doi: 10.1177/0885328219898385.

Final publication is available from Mary Ann Liebert, Inc.: https://doi.org/10.1089/3dp.2022.0235

31. Schaedler TA, Jacobsen AJ, Torrents A, et al. Ultralight Metallic Microlattices. Science 2011;334(6058):962–965; doi: 10.1126/science.1211649.

32. Silverstein MS and Cameron NR. PolyHIPEs - Porous Polymers from High Internal Phase Emulsions. Encyclopedia of Polymer Science and Technology. 2002.

33. Silverstein MS. Emulsion-Templated Polymers: Contemporary Contemplations. Polymer 2017;126:261–282; doi: 10.1016/j.polymer.2017.07.046.

34. Kramer S, Cameron NR, Krajnc P. Porous polymers from high internal phase emulsions as scaffolds for biological applications. Polymers 2021;13(11):1786; doi: 10.3390/polym13111786.

35. Luo J, Huang Z, Liu L, et al. Recent Advances in Separation Applications of Polymerized High Internal Phase Emulsions. J Sep Sci 2021;44(1):169–187; doi: 10.1002/jssc.202000612.

36. Choi JS, Kang HW, Lee IH, et al. Development of Micro-Stereolithography Technology Using a UV Lamp and Optical Fiber. Int J Adv Manuf Syst 2009;41(3):281–286; doi: 10.1007/s00170-008-1461-1.

37. Han LH, Mapili G, Chen S, et al. Freeform Fabrication of Biological Scaffolds by Projection Photopolymerization. In: 2007 International Solid Freeform Fabrication Symposium. 2007;450–457.

38. Sušec M, Ligon SC, Stampfl J, et al. Hierarchically Porous Materials from Layer-by-Layer Photopolymerization of High Internal Phase Emulsions. Macromol Rapid Commun 2013;34(11):938–943; doi: 10.1002/marc.201300016.

Final publication is available from Mary Ann Liebert, Inc.: https://doi.org/10.1089/3dp.2022.0235

SUPPLEMENTARY DATA

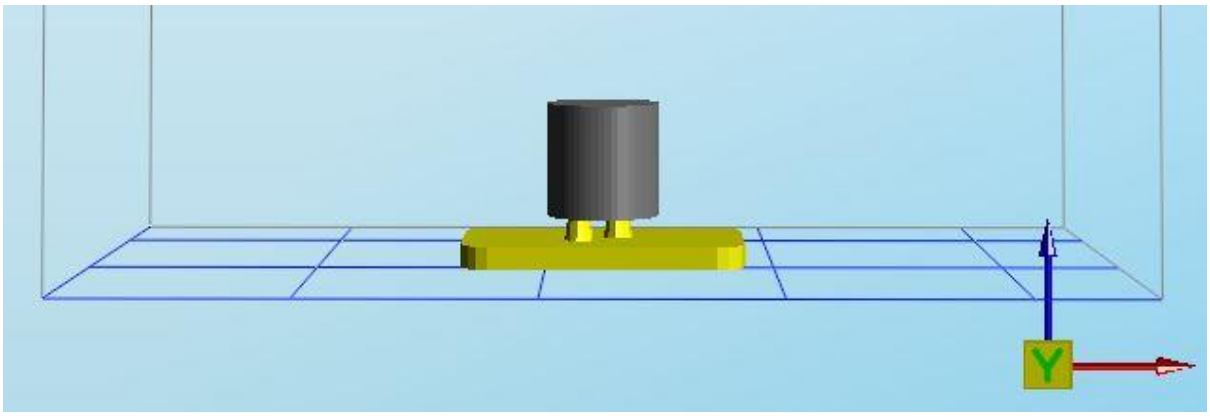

Figure 1. *The 3D model of 5×5 mm cylinder*

Table 1. *Printing parameters to 3D print 5×5 mm cylinders from pure HIPE*

From layer	To layer	Exposure time (sec)	Lifting height (mm)	Lifting speed (mm/min)	Down speed (mm/min)	Delay time (sec)
1	1	35	5	10	40	0.3
2	32	27	5	10	40	0.3
33	66	22	5	10	40	0.3
67	125	17	5	15	40	0.3
126	175	13	5	15	40	0.3
176	200	9	5	15	40	0.3
201	225	6	5	15	40	0.3
226	233	4	5	15	40	0.3

Final publication is available from Mary Ann Liebert, Inc.: https://doi.org/10.1089/3dp.2022.0235

Table 2. *Printing parameters to 3D print 5×5 mm cylinders from HIPE that contained 0.4% beta-carotene*

From layer	To layer	Exposure time (sec)	Lifting height (mm)	Lifting speed (mm/min)	Down speed (mm/min)	Delay time (sec)
1	1	40	5	10	40	0.3
2	32	37	5	10	40	0.3
33	66	35	5	10	40	0.3
67	125	32	5	15	40	0.3
126	175	30	5	15	40	0.3
176	200	25	5	15	40	0.3
201	225	20	5	15	40	0.3
226	233	15	5	15	40	0.3

Table 3. *Printing parameters to 3D print 5×5 mm cylinders from HIPE that contained 0.1% tartrazine*

From layer	To layer	Exposure time (sec)	Lifting height (mm)	Lifting speed (mm/min)	Down speed (mm/min)	Delay time (sec)
1	1	40	5	10	40	0.3
2	32	39	5	10	40	0.3
33	66	37	5	10	40	0.3
67	125	34	5	15	40	0.3
126	175	32	5	15	40	0.3
176	200	27	5	15	40	0.3
201	225	22	5	15	40	0.3
226	233	17	5	15	40	0.3

Final publication is available from Mary Ann Liebert, Inc.: https://doi.org/10.1089/3dp.2022.0235

Table 4. *Printing parameters to 3D print 5×5 mm cylinders from HIPE that contained blend (0.4% beta-carotene and 0.1% tartrazine)*

From layer	To layer	Exposure time (sec)	Lifting height (mm)	Lifting speed (mm/min)	Down speed (mm/min)	Delay time (sec)
1	1	40	5	10	40	0.3
2	32	37	5	10	40	0.3
33	66	35	5	10	40	0.3
67	125	32	5	15	40	0.3
126	175	30	5	15	40	0.3
176	200	25	5	15	40	0.3
201	225	20	5	15	40	0.3
226	233	15	5	15	40	0.3

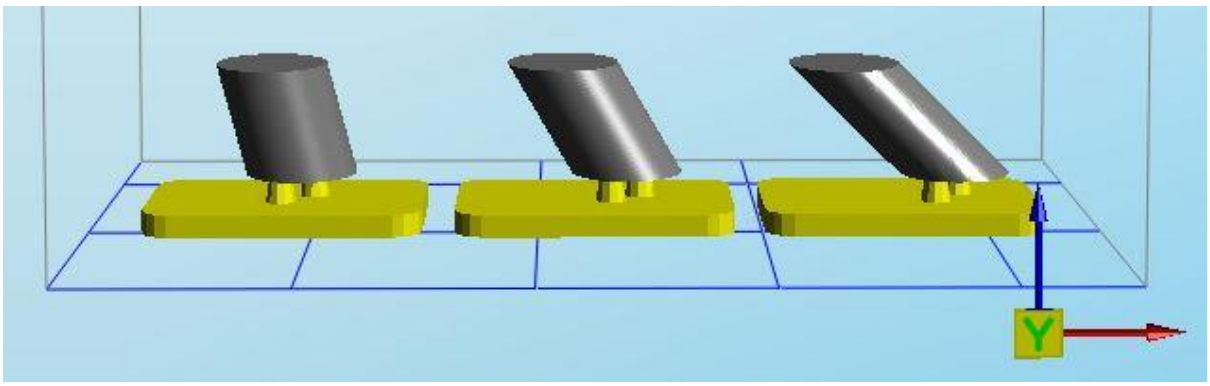

Figure 2. *The 3D model of 5×5 mm cylinders having 15°, 30°, and 45° inclines*

Final publication is available from Mary Ann Liebert, Inc.: https://doi.org/10.1089/3dp.2022.0235

Table 5. *Printing parameters to 3D print 5×5 mm cylinders having 15°, 30°, and 45° inclines from pure HIPE*

From layer	To layer	Exposure time (sec)	Lifting height (mm)	Lifting speed (mm/min)	Down speed (mm/min)	Delay time (sec)
1	1	35	5	10	40	0.3
2	32	27	5	10	40	0.3
33	66	22	5	10	40	0.3
67	125	17	5	15	40	0.3
126	175	13	5	15	40	0.3
176	200	9	5	15	40	0.3
201	225	6	5	15	40	0.3
226	233	4	5	15	40	0.3

Table 6. *Printing parameters to 3D print 5×5 mm cylinders having 15°, 30°, and 45° inclines from HIPE that contained 0.4% beta-carotene*

From layer	To layer	Exposure time (sec)	Lifting height (mm)	Lifting speed (mm/min)	Down speed (mm/min)	Delay time (sec)
1	1	45	5	10	40	0.3
2	32	40	5	10	40	0.3
33	66	35	5	10	40	0.3
67	125	32	5	15	40	0.3
126	175	28	5	15	40	0.3
176	200	24	5	15	40	0.3
201	225	19	5	15	40	0.3
226	233	15	5	15	40	0.3

Final publication is available from Mary Ann Liebert, Inc.: https://doi.org/10.1089/3dp.2022.0235

Table 7. *Printing parameters to 3D print 5×5 mm cylinders having 15°, 30°, and 45° inclines from HIPE that contained 0.1% tartrazine*

From layer	To layer	Exposure time (sec)	Lifting height (mm)	Lifting speed (mm/min)	Down speed (mm/min)	Delay time (sec)
1	1	60	5	10	40	0.3
2	76	57	5	10	40	0.3
77	150	55	5	10	40	0.3
151	225	53	5	15	40	0.3
226	233	50	5	15	40	0.3

Table 8. *Printing parameters to 3D print 5×5 mm cylinders having 15°, 30°, and 45° inclines from HIPE that contained blend (0.4% beta-carotene and 0.1% tartrazine)*

From layer	To layer	Exposure time (sec)	Lifting height (mm)	Lifting speed (mm/min)	Down speed (mm/min)	Delay time (sec)
1	1	45	5	10	40	0.3
2	32	42	5	10	40	0.3
33	66	38	5	10	40	0.3
67	125	34	5	15	40	0.3
126	175	29	5	15	40	0.3
176	200	26	5	15	40	0.3
201	225	22	5	15	40	0.3
226	233	18	5	15	40	0.3

Final publication is available from Mary Ann Liebert, Inc.: https://doi.org/10.1089/3dp.2022.0235

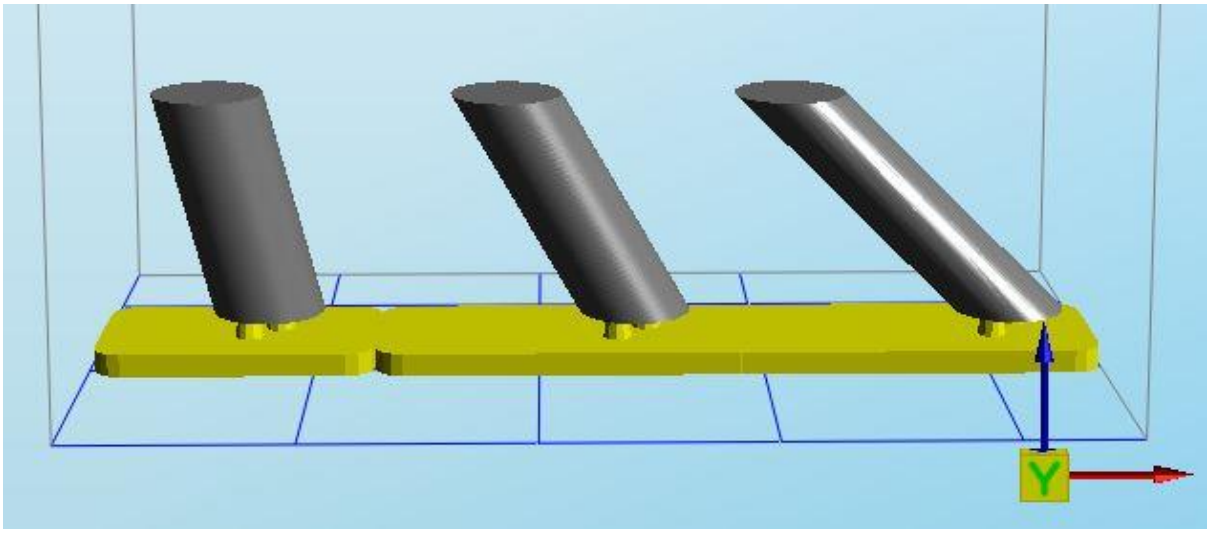

Figure 3. *The 3D model of 5×10 mm cylinders having 15°, 30°, and 45° inclines*

Table 9. *Printing parameters to 3D print 5×10 mm cylinders having 15°, 30°, and 45° inclines from pure HIPE*

From layer	To layer	Exposure time (sec)	Lifting height (mm)	Lifting speed (mm/min)	Down speed (mm/min)	Delay time (sec)
1	1	35	5	10	40	0.3
2	32	27	5	10	40	0.3
33	76	22	5	10	40	0.3
77	150	17	5	15	40	0.3
151	225	13	5	15	40	0.3
226	300	9	5	15	40	0.3
301	370	6	5	15	40	0.3
371	411	4	5	15	40	0.3

Final publication is available from Mary Ann Liebert, Inc.: https://doi.org/10.1089/3dp.2022.0235

Table 10. *Printing parameters to 3D print 5×5 mm cylinders having 15°, 30°, and 45° inclines from HIPE that contained 0.4% beta-carotene*

From layer	To layer	Exposure time (sec)	Lifting height (mm)	Lifting speed (mm/min)	Down speed (mm/min)	Delay time (sec)
1	1	45	5	10	40	0.3
2	32	42	5	10	40	0.3
33	76	38	5	10	40	0.3
77	150	35	5	15	40	0.3
151	225	32	5	15	40	0.3
226	300	28	5	15	40	0.3
301	370	24	5	15	40	0.3
371	411	20	5	15	40	0.3

Table 11. *Printing parameters to 3D print 5×5 mm cylinders having 15°, 30°, and 45° inclines from HIPE that contained blend (0.4% beta-carotene and 0.1% tartrazine)*

From layer	To layer	Exposure time (sec)	Lifting height (mm)	Lifting speed (mm/min)	Down speed (mm/min)	Delay time (sec)
1	1	45	5	10	40	0.3
2	32	42	5	10	40	0.3
33	76	38	5	10	40	0.3
77	150	35	5	15	40	0.3
151	225	32	5	15	40	0.3
226	300	28	5	15	40	0.3
301	370	24	5	15	40	0.3
371	411	20	5	15	40	0.3

Final publication is available from Mary Ann Liebert, Inc.: https://doi.org/10.1089/3dp.2022.0235

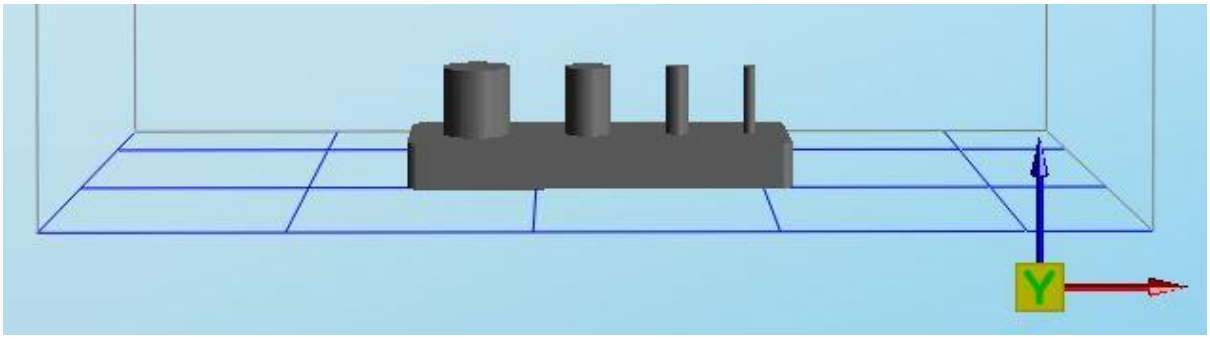

Figure 4. *The 3D model of calibration object including 5 mm high posts of 3 mm, 2 mm, 1 mm, and 0.5 mm diameters*

Table 12. *Printing parameters to 3D print calibration object including 5 mm high posts of 3 mm, 2 mm, 1 mm, and 0.5 mm diameters from pure HIPE*

From layer	**To layer**	**Exposure time (sec)**	**Lifting height (mm)**	**Lifting speed (mm/min)**	**Down speed (mm/min)**	**Delay time (sec)**
1	1	35	5	10	40	0.3
2	32	27	5	10	40	0.3
33	64	22	5	10	40	0.3
65	100	17	5	15	40	0.3
101	125	13	5	15	40	0.3
126	150	9	5	15	40	0.3
151	163	6	5	15	40	0.3

Final publication is available from Mary Ann Liebert, Inc.: https://doi.org/10.1089/3dp.2022.0235

Table 13. *Printing parameters to 3D print calibration object including 5 mm high posts of 3 mm, 2 mm, 1 mm, and 0.5 mm diameters from HIPE that contained 0.4% beta-carotene*

From layer	To layer	Exposure time (sec)	Lifting height (mm)	Lifting speed (mm/min)	Down speed (mm/min)	Delay time (sec)
1	1	40	5	10	40	0.3
2	32	37	5	10	40	0.3
33	64	35	5	10	40	0.3
65	100	32	5	15	40	0.3
101	125	30	5	15	40	0.3
126	150	25	5	15	40	0.3
151	163	20	5	15	40	0.3

Table 14. *Printing parameters to 3D print calibration object including 5 mm high posts of 3 mm, 2 mm, 1 mm, and 0.5 mm diameters from HIPE that contained 0.1% tartrazine*

From layer	To layer	Exposure time (sec)	Lifting height (mm)	Lifting speed (mm/min)	Down speed (mm/min)	Delay time (sec)
1	1	42	5	10	40	0.3
2	32	39	5	10	40	0.3
33	64	37	5	10	40	0.3
65	100	34	5	15	40	0.3
101	125	32	5	15	40	0.3
126	150	27	5	15	40	0.3
151	163	22	5	15	40	0.3

Final publication is available from Mary Ann Liebert, Inc.: https://doi.org/10.1089/3dp.2022.0235

Table 15. *Printing parameters to 3D print calibration object including 5 mm high posts of 3 mm, 2 mm, 1 mm, and 0.5 mm diameters from HIPE that contained blend (0.4% beta-carotene and 0.1% tartrazine)*

From layer	To layer	Exposure time (sec)	Lifting height (mm)	Lifting speed (mm/min)	Down speed (mm/min)	Delay time (sec)
1	1	40	5	10	40	0.3
2	32	37	5	10	40	0.3
33	64	35	5	10	40	0.3
65	100	32	5	15	40	0.3
101	125	30	5	15	40	0.3
126	150	25	5	15	40	0.3
151	163	20	5	15	40	0.3

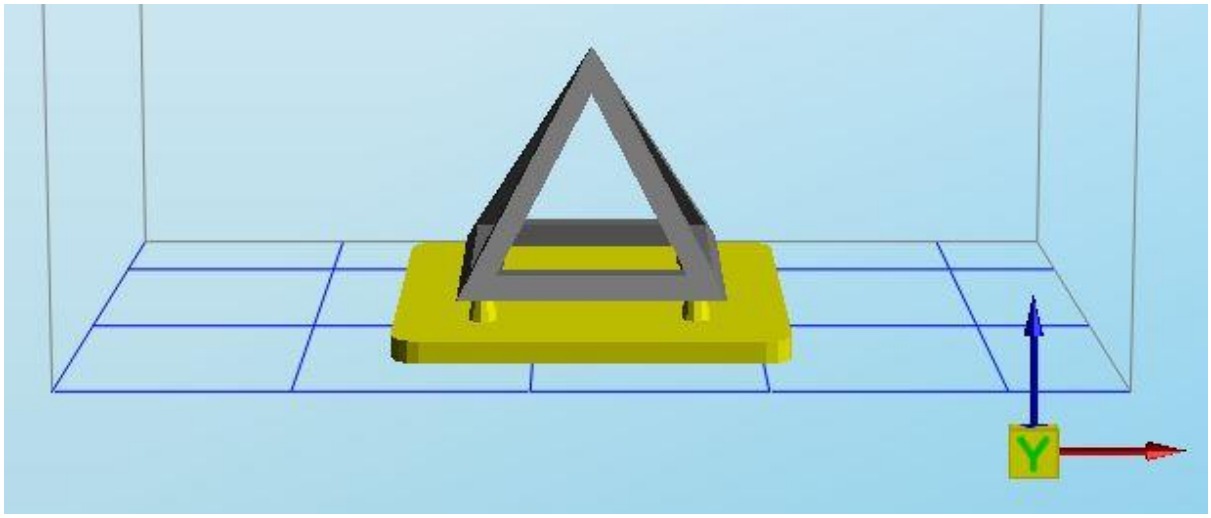

Figure 5. *The 3D model of pyramid structure*

Final publication is available from Mary Ann Liebert, Inc.: https://doi.org/10.1089/3dp.2022.0235

Table 16. *Printing parameters to 3D print pyramid structure from pure HIPE that contained blend (0.4% beta-carotene and 0.1% tartrazine)*

From layer	**To layer**	**Exposure time (sec)**	**Lifting height (mm)**	**Lifting speed (mm/min)**	**Down speed (mm/min)**	**Delay time (sec)**
1	1	40	5	10	40	0.3
2	32	37	5	10	40	0.3
33	66	35	5	10	40	0.3
67	125	32	5	15	40	0.3
126	200	30	5	15	40	0.3
201	275	25	5	15	40	0.3
276	310	20	5	15	40	0.3
311	341	15	5	15	40	0.3

Final publication is available from Mary Ann Liebert, Inc.: https://doi.org/10.1089/3dp.2022.0235

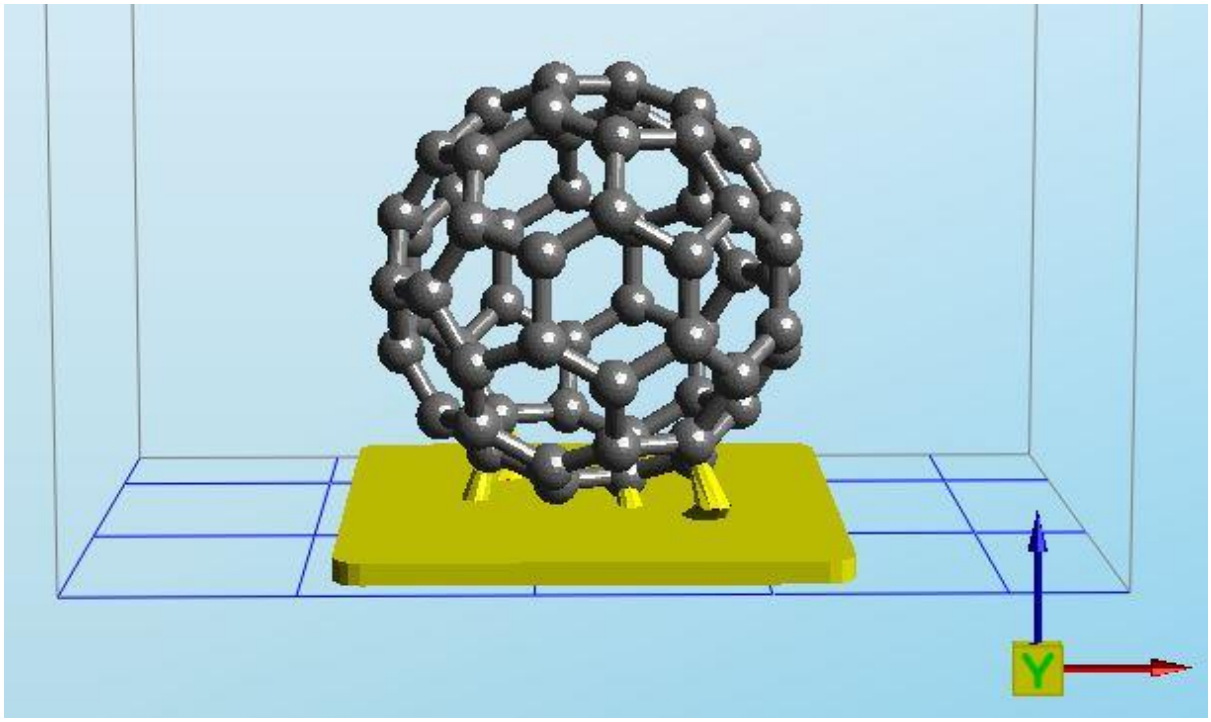

Figure 6. *The 3D model of buckyball structure*

Final publication is available from Mary Ann Liebert, Inc.: https://doi.org/10.1089/3dp.2022.0235

Table 17. *Printing parameters to 3D print buckyball structure from pure HIPE that contained blend (0.4% beta-carotene and 0.1% tartrazine)*

From layer	**To layer**	**Exposure time (sec)**	**Lifting height (mm)**	**Lifting speed (mm/min)**	**Down speed**	**Delay time**
1	1	50	5	10	40	0.3
2	32	47	5	10	40	0.3
33	66	43	5	10	40	0.3
67	250	40	5	10	40	0.3
251	350	37	5	10	40	0.3
351	420	33	5	10	40	0.3
421	500	29	5	10	40	0.3
501	570	25	5	15	40	0.3
571	600	22	5	15	40	0.3
601	680	20	5	15	40	0.3
681	712	17	5	15	40	0.3

Final publication is available from Mary Ann Liebert, Inc.: https://doi.org/10.1089/3dp.2022.0235

Table 18. *Print times of 3D model for each HIPE category*

3D model	Print time (pure)	Print time (0.4% beta-carotene)	Print time (0.1% tartrazine)	Print time (blend)
5×5 mm cylinders	2 h 59 min	3 h 55 min	4 h 2 min	3 h 55 min
5×5 mm cylinders having 15°, 30°, and 45° inclines	2 h 59 min	3 h 55 min	3 h 35 min	4 h 2 min
5×10 mm cylinders having 15°, 30°, and 45° inclines	4 h 55 min	6 h 55 min	9 h 5 min	6 h 55 min
Calibration object	2 h 13 min	2 h 52 min	2 h 57 min	2 h 52 min
Pyramid	-	-	-	5 h 27 min
Buckyball	-	-	-	13 h 19 min

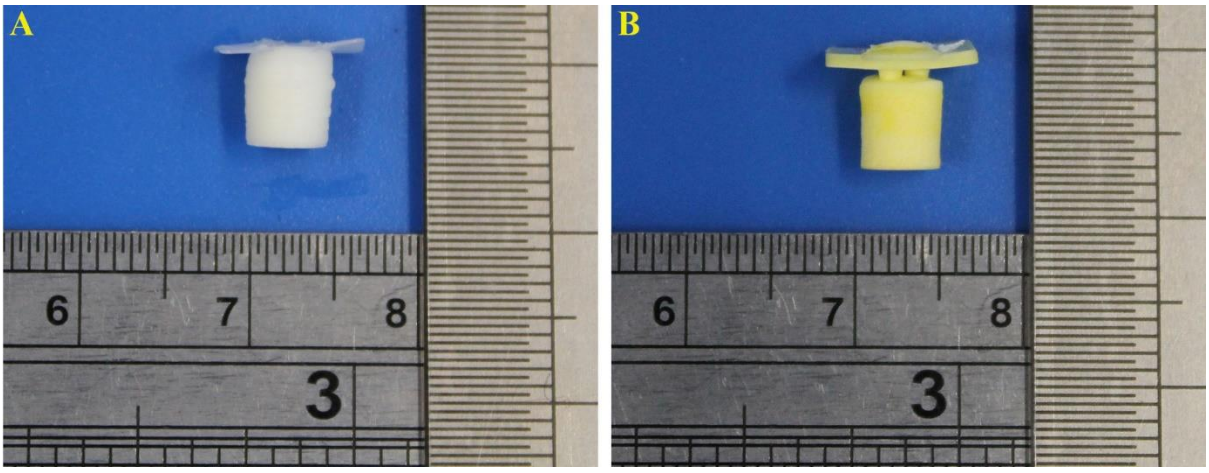

Figure 7. *The comparison of the* ***(A)*** *pure and* ***(B)*** *blend samples in terms of overcuring*

Final publication is available from Mary Ann Liebert, Inc.: https://doi.org/10.1089/3dp.2022.0235

Table 19. *Diameter and height values of the pure and blend samples before and after drying*

Samples	Before drying		After drying	
	d (mm)	**h (mm)**	**d (mm)**	**h (mm)**
Pure	4.78 ± 0.11	5.17 ± 0.04	4.67 ± 0.18	4.94 ± 0.12
Blend	4.82 ± 0.09	4.93 ± 0.04	4.72 ± 0.06	4.86 ± 0.06